INSTITUTE OF PHYSICS PUBLISHING JOURNAL OF PHYSICS B: ATOMIC, MOLECULAR AND OPTICAL PHYSICS

J. Phys. B: At. Mol. Opt. Phys. **34** (2001) 3717–3726 PII: S0953-4075(01)25041-X

XUV diagnostics of colliding laser-produced magnesium plasmas

S S Harilal[1,3], **C V Bindhu**[1,3], **V P Shevelko**[2] **and H-J Kunze**[1]

[1] Ruhr-Universitaet Bochum, Institut fuer Experimentalphysik V, Universitaetsstrasse 150, D-44780 Bochum, Germany
[2] P N Lebedev Physics Institute, Russian Academy of Sciences, Moscow 117924, Russia

E-mail: harilal@fusion.ucsd.edu and kunze@ep5.ruhr-uni-bochum.de

Received 16 May 2001, in final form 13 July 2001
Published 10 September 2001
Online at stacks.iop.org/JPhysB/34/3717

Abstract

Charge exchange collisions between highly charged Mg ions in colliding laser-produced magnesium plasmas are studied. Pinhole photography and XUV spectroscopy are used as diagnostic tools. XUV pinhole pictures taken at early stages give more insight into the expansion dynamics of the colliding magnesium plasmas. Spectroscopic studies show selective population of the $n = 3$ levels of Mg IX ions which results in enhancement of respective line intensities. Theoretical calculations also give large cross section as high as 10^{-15} cm^2 for these charge exchange collisions when the relative velocities of the colliding ions are of the order of 10^7 cm s^{-1}.

1. Introduction

Lasers have been extensively used for the ablation of solid materials and the number of applications is still increasing [1, 2]. To understand the process of laser ablation requires an understanding of the initial stages of various processes involved during laser–target interaction, i.e. evaporation, plasma formation, and its subsequent expansion into vacuum or ambient gas [3, 4]. There are several diagnostic techniques for characterizing a laser-produced plasma, and these include optical emission spectroscopy [5, 6], mass spectroscopy [7, 8], VUV/XUV absorbance spectroscopy [9], laser-induced fluorescence (LIF) [10], Langmuir probes [11, 12], microwave and laser interferometry [13, 14], Thomson scattering [15], etc. Fast photography and other imaging techniques add another dimension to ablation diagnostics by providing two-dimensional snap shots of the three-dimensional plume propagation [16]. This capability becomes essential for understanding the hydrodynamics of the plume propagation and reactive scattering.

[3] Present address: Center for Energy Research, University of California San Diego, CA 92093-0417, USA.

Several applications of laser-produced plasmas involve an experimental situation where plasmas collide. Laser-produced colliding plasmas find potentially attractive applications in the field of x-ray lasers, in stimulated Raman scattering experiments, and they are of relevance for the design of inertial confinement fusion (ICF) hohlraums [17–19]. In addition to these applications, the interpenetration of two plasmas occurs also in astrophysical systems, for example after a super nova explosion ejects plasma into the interstellar medium, when releasing barium into the solar wind, or in the interaction of comets with the solar wind [20,21]. Recently high Mach number radiatively cooled jets relevant to astrophysical jets were produced during collapse of laser-produced plasmas using a conically shaped target [22, 23]. Despite considerable experimental and theoretical progress in the dynamics of single laser-produced plasmas, little attention has been paid to the study of the nature and of the dynamics of laser-produced colliding plasmas. Moreover, most of the colliding plasma experiments were carried out employing high-intensity lasers ($>10^{13}$ W cm^{-2}) [19, 24]. However, experiments with low-intensity lasers are extremely valuable for elucidating underlying science. Previous experiments have incorporated a variety of beam–target configurations including dual beam and parallel planar targets [25], split beam and single planar target [26], split beam and target slabs placed orthogonally [27], single beam and internally irradiated microtubes [28]. In conjunction with experimental studies, numerical modelling has been able to reproduce observed features of the plasma, such as the temperature, density and emissivity [29].

When two streaming plasmas collide various interactions can arise. These may be of collisionless type in which case collective plasma effects occur or they are collision dominated. Depending upon collisionality of the plasmas, which in turn depends on temperature, density and ionic charge, varying amounts of interpenetration are predicted [19]. In this paper we report the characteristics of colliding laser-produced magnesium plasmas studied using XUV photography and XUV spectroscopy. We specifically investigate the possibility for charge exchange collisions between ions of hot and cold plasma.

2. Experimental set-up

A schematic diagram of the experimental set-up is given in figure 1(*a*). A pulse from a ruby laser (6 J, 15 ns) is split into two beams with different intensities by means of a movable glass wedge (figure 1(*b*)). Changing the position of the wedge can vary the intensity ratio of the two beams. These two beams are focussed by a plano-convex lens with a focal length $f = 300$ mm onto two magnesium slabs placed at 90° to each other (figure 1(*c*)) that are kept in a vacuum chamber. The target slabs are placed on a motorized linear mount so that fresh surface is presented to the laser for each shot. This prevents the creation of craters that will occlude emission from the hot core of the plasma. The relation gives the distance between the two foci at the target surface

$$d = f\gamma(n-1) \tag{1}$$

where $n = 1.5$, the refractive index; γ is the acute angle of the wedge. In the present studies we used a glass wedge with an acute angle of 17′02″ which corresponds to a distance of separation between the foci of $d = 0.75$ mm. The estimated spot sizes on the target surface were approximately 400 μm. The images of the plume were obtained in a single shot mode with a gated charged-coupled device (CCD) camera intensified by a microchannel plate (MCP) whose opening was delayed by a pulse generator triggered by the laser shot. For the XUV pinhole camera we used a 50 μm pinhole with an aluminium filter (27 mg cm^{-3}), resulting in a spectral sensitivity of the system of <80 nm. The pinhole pictures were taken from a direction perpendicular to the plane of the two laser beams.

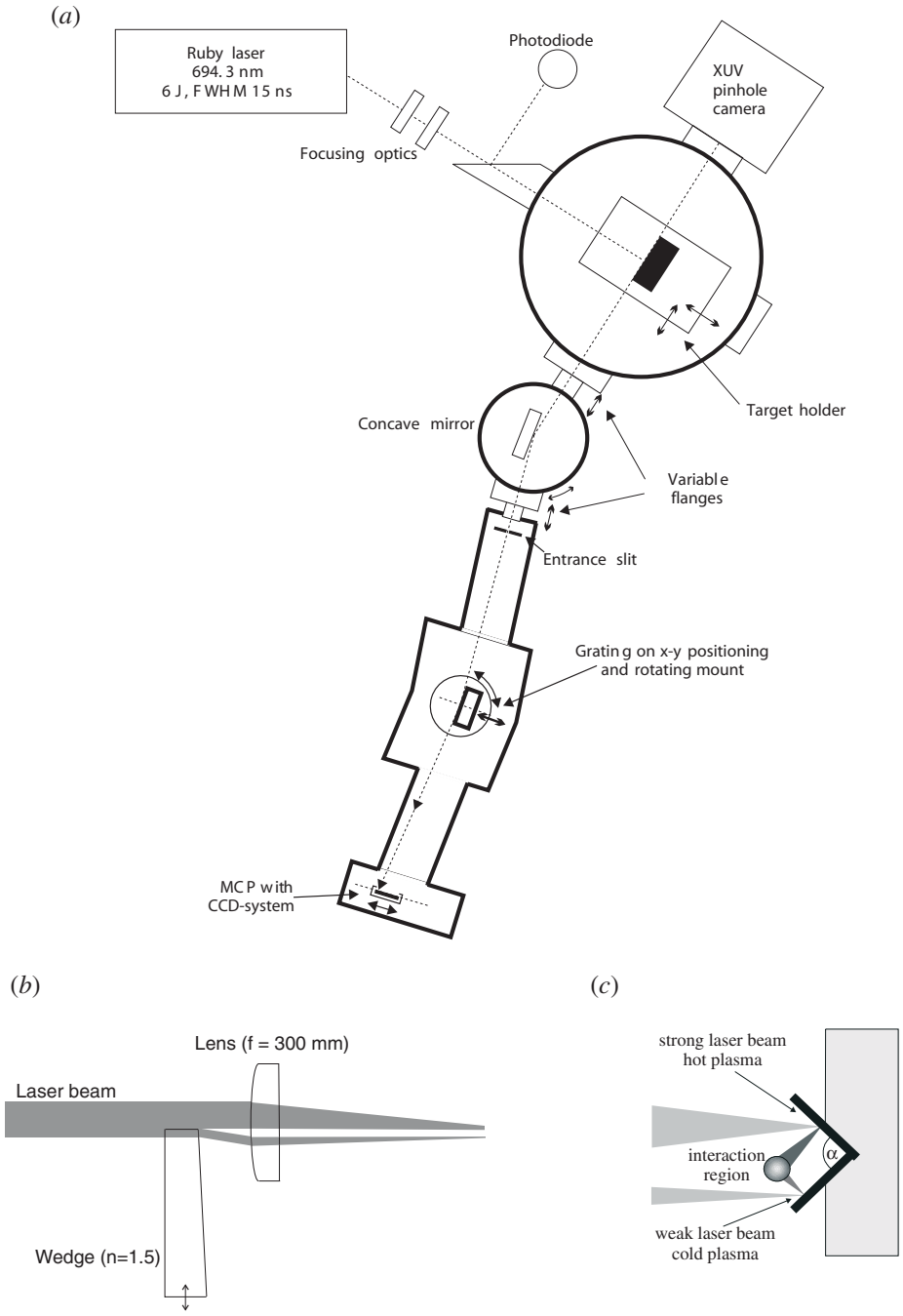

Figure 1. (*a*) Schematic diagram of the experimental set-up used for the XUV spectral studies. (*b*) Wedge and lens combination which are used for splitting the laser beam. (*c*) Target geometry used for the present studies.

For spectral studies, a gold-coated spherical mirror with 4 m radius of curvature was used to image the emitted radiation onto the entrance slit of the grazing incidence spectrograph. This set-up essentially provided spatial resolution to better than 200 μm. The spectrograph was equipped with a concave grating with a 5649 mm radius of curvature and set for an angle of incidence on the grating of 87°. The gold plated grating with varying groove spacing (1095–1450 lines/mm) focused the spectrum on a flat plane instead of on the Rowland circle. The spectrograph covers the spectral range from 3–25 nm at moderate wavelength resolution (typically $\lambda/\Delta\lambda = 100$ at a slit width of 10 μm). To detect soft x-rays in the 3–12 nm wavelength range, we employed the same MCP–CCD assembly used for the imaging studies. The CCD detector was connected to a computer equipped with software for data acquisition and spectral analysis. The wavelength calibration of the monochromator was carried out by plasma spectroscopy using a carbon target. The pinhole imaging and recording of the XUV spectra were done separately.

3. Results and discussion

3.1. Pinhole pictures

XUV pinhole pictures of plasmas reveal more details about expansion dynamics of the plasma plume. As XUV radiation is emitted only by hot and dense plasma where higher ionization stages dominate, this technique is suitable for studying the plasma plume in the earlier stages [14]. In the present experiment, the targets are mounted at an angle of 90° to each other. This arrangement leads to a good interpenetration of the two plasmas because of higher relative velocities than in the case of laterally colliding plasmas [30]. The intensity ratio of the two laser beams is 7:1, which gives power densities of 2×10^{11} W cm^{-2} and 3×10^{10} W cm^{-2}, respectively at the focal spots. The positions of the foci of the hot and the cold plasmas on the target surfaces are very important parameters because this governs the relative velocity with which the plasmas collide. In order to account for the higher expansion velocity of the hot plasma, the hot laser spot is placed closer to the common edge compared to the weak beam spot. A slight change in the geometry causes drastic changes in the shape and position of the interaction region. The targets are placed on a motorized translator so that we can move the targets in a direction perpendicular to the laser beam. Extra care has been taken during translation so that target geometry remains undisturbed. The plume images are recorded by producing colliding plasma from two extreme positions (within the limit of the translator movement) of the target geometry. Both the images are found to be similar indicating the interaction region of the colliding plasma.

Figure 2 gives pinhole pictures taken at different times after the maximum of the laser pulse. The bright plume in the upper part of the image is the hot plasma and the plume in the lower part is the cold plasma. For these studies the MCP was gated with 5 ns. The expansion velocities of both plasmas are measured from the time evolution of the pinhole pictures. The estimated expansion velocities of hot and cold plasma in the initial stages are $(6 \pm 2) \times 10^6$ and $(3 \pm 1) \times 10^6$ cm s^{-1}, respectively. Initially both plasmas expand freely. As time evolves, a thin interaction region (about 75 μm thick) begins to evolve at the collision region of the two plasmas and the intensity of the interaction region becomes brighter with time. It is interesting to note that the thickness of the interaction region becomes wider as time elapses. The length of the interaction region becomes $\sim$1 mm (including penumbral image) at 15 ns after the laser maximum. At later times the collision region is found to be tilted towards the direction of the hot plasma (anticlockwise). The tilting of the collision region is expected to be due to the lower expansion velocity of the plasmas at the outer region of the target. At times greater than

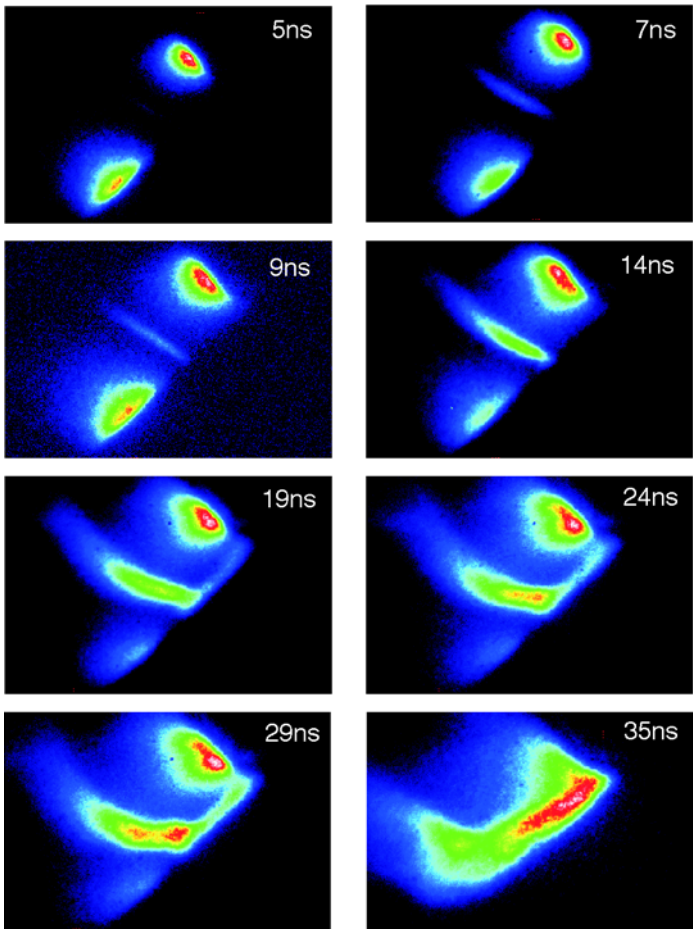

Figure 2. Time evolution of colliding plasmas recorded using a 50 μm pinhole camera. The time given in the pictures is the delay of the gate pulse after the laser pulse maximum. The gate width was set at 5 ns. The foci were separated by a distance of 0.75 mm.

(This figure is in colour only in the electronic version)

30 ns, a radiating region appears also at the target slab close to the hot plasma: this can be understood as the high energetic ions and electrons from the hot plasma hit the target surface, which in turn creates a secondary plasma near the hot plasma. We observed such a radiation region with hot plasma alone. Finally, this secondary plasma also interacts with oncoming plasma, which leads to a brighter emission from the collision region (figure 2, 35 ns).

Figure 3 represents the temporal evolution of the maximum brightness (taken from the image) of the three plasma clouds (namely, hot, cold and colliding) with time elapsed after the maximum of the laser pulse. It is observed that the emission intensities of hot and cold plasmas increase up to a certain time and then decrease with time. The colliding region appears with a delay after the maximum of the laser pulse. The overall intensity of the colliding plasma is found to enhance with time and peaks around 20 ns after the maximum of the laser pulse. It is worth noticing that the plume intensity of the colliding region is higher at later times than that of the hot and cold plasma.

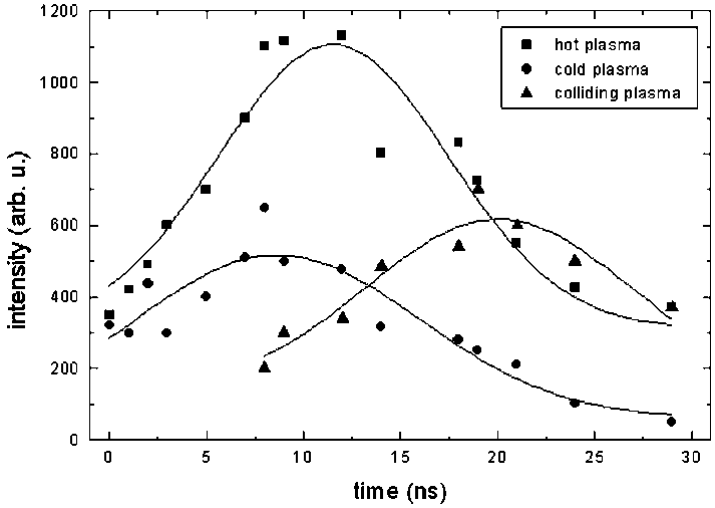

Figure 3. The temporal evolution of the brightness taken from the pinhole pictures of the three plasma clouds (namely, hot, cold and colliding) with time elapsed after the maximum of the laser pulse. At later times, the intensity of the colliding region is higher than that of the single plasmas.

As the plasma expands from the solid surface it rapidly cools. Its outward expansion velocities are large. For sufficiently low plasma densities where the ion–ion mean free path exceeds the dimensions of the system, the two plasmas interpenetrate with little collisional interaction. Interpenetration of the plasmas takes place at short times (<1 ns) and during interpenetration the population density is perturbed by charge exchange collisions. At high plasma densities, where the ion–ion mean free path is smaller than the plasma density scale lengths, the region of plasma interpenetration is relatively small. In this case, the plasmas stagnate. For colliding plasmas with relatively large velocity and/or low density, interpenetration is expected, leading to a wide heated region building up at relatively later times, and in the case of low relative velocity and/or high density, the plasmas will collide and stop almost immediately, leading to a very localized heated region. A recent paper [24] describing the experimental study of the collision of aluminium plasma with magnesium plasma confirms that the plasmas interpenetrate each other at early times and stagnate at later times. When these plasmas collide the directed kinetic energy can be converted into thermal energy, the plasmas heat up and slow down. The relative velocity of the plasmas will be reduced by the interaction and the momentum transfer cross sections increased. This in turn will create a rapid build-up of stationary plasma in the interaction region.

3.2. XUV spectral studies

Spectroscopic studies are needed in the present case to find out whether the emission of the collision zone is due to stagnation of the plasmas or if the plasmas interpenetrate and show stronger emission due to charge exchange collisions. XUV spectra are taken in the spectral range 3–10 nm using a grazing incidence spectrograph. Figures 4(*a*) and (*b*) gives such spectra for colliding, hot and cold plasmas. These spectra are taken at a distance of 0.8 mm from the common edge of the targets and 8 ns after the maximum of the laser pulse. The MCP was gated for 10 ns for the spectral studies. We have not observed any emission due to cold plasma in the spectral range 3–6 nm. In the case of hot and colliding plasmas, it is noted that at shorter

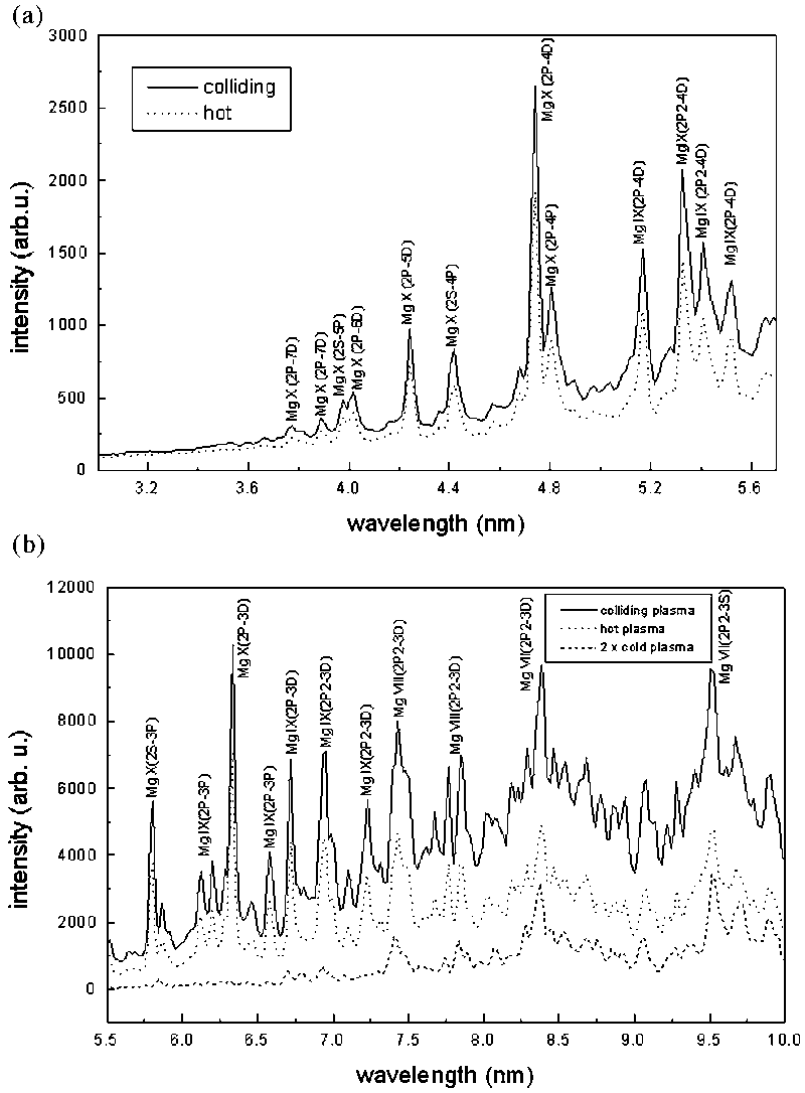

Figure 4. Spectra of colliding, hot and cold plasmas. (*a*) Spectra in the wavelength range 3–6 nm. In this region, the emission due to cold plasma was not observed. (*b*) Spectra in the wavelength region 6–12 nm. The spectra were taken at a distance 0.8 mm from the common edge of the target and with a gate width of 10 ns.

wavelengths (3–6 nm), the spectra are dominated by emission due to Li-like (Mg x) and Be-like (Mg ix) magnesium ions whereas emission from ions like Mg viii and Mg vii dominates the higher wavelength region of the spectrum.

In the case of colliding plasmas, a strong continuum emission is observed. This continuum emission scales by a factor two over the whole spectral range indicating, to a first approximation, an electron density increase of about 40–50%. The enhancement in the continuum intensity centred around 8 nm is a result of the enhancement in free–free bremsstrahlung and electron–ion recombination. In order to illustrate the variation of total line intensities, the intensity ratio of the emitted spectral lines from colliding plasmas with respect to those of the single hot plasma

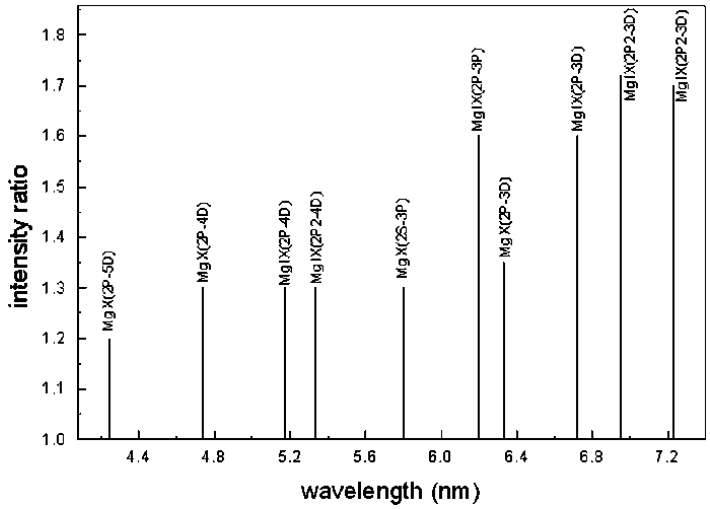

Figure 5. Intensity ratio of Li-like and Be-like lines from colliding plasmas with lines from hot plasma.

after subtracting the continuum is given in figure 5 for lithium-like (Mg x) and beryllium-like (Mg ix) magnesium. We observe enhancement of the line intensities for different ionic lines and it is predominant for lines originating from $n = 3$ levels of beryllium-like magnesium, even if it is comparatively not very large. At the red end of the observed spectra (not given in figure 5), the enhancement in the intensities of all emission of lower ionization stages lines is about a factor two. This is certainly due to recombination.

There are only a very few reports that describe the plasma interpenetration and charge exchange collisions in laser-produced colliding plasmas. Recently, Ruhl *et al* [27] investigated the possibility of charge exchange collisions in a colliding laser-produced carbon plasma and they observed selective population of the $n = 3$ level of hydrogen-like carbon due to charge exchange collisions between C vii and C iii. Rancu *et al* [31] studied the collision of two plasmas produced from laser-exploded Al/Al and Al/Mg foils by x-ray diagnostics over a wide range of experimental conditions. Their experimental data along with simulations gave a good understanding of the localization and dynamics of the kinetic to thermal energy transfer in the interpenetration region. Wan *et al* [19] used soft x-ray laser interferometer for studying the collision and subsequent interaction of counter streaming high-density plasmas. Their electron density measurements showed the evolution of the counter streaming plasmas from interpenetration at early time to stagnation at later times. Bosch *et al* [25] investigated the collision and interpenetration of plasmas produced during laser ablation of two parallel discs made of aluminium and magnesium, respectively. Time integrated spatially and spectrally resolved emission in the x-ray region provided direct evidence of interpenetration, stagnation and ion thermalization.

We observe an enhancement in the intensity for lines originating from the $n = 3$ levels of beryllium-like magnesium ions. The intensity enhancement for lines originating from $n \geqslant 4$ is less evident in the observed spectra. The electron-capture cross sections have been calculated by a multichannel normalization procedure of the capture probability in the impact parameter representation using the hydrogen-like wavefunctions for both the target and the incident ion. Calculations have been performed for charge exchange cross sections for different ions by the computer code CAPTURE described in the paper by Tolstikhina and Shevelko [32, 33].

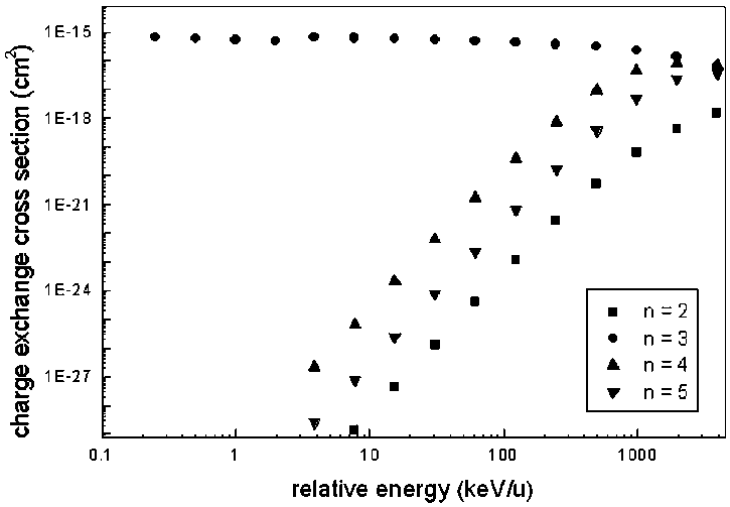

Figure 6. Calculated charge exchange cross sections as a function of relative energy into different n levels of Mg IX. It shows charge exchange cross sections are very high for lines originating from $n = 3$ level irrespective of relative energy of collision between Mg X and Mg V.

Calculations show large cross sections for the following charge exchange process for lines originated from the $n = 3$ level:

$$\text{Mg X} + \text{Mg V} \rightarrow \text{Mg IX} + \text{Mg VI}. \tag{2}$$

Figure 6 shows these theoretical cross sections into different n levels of Mg IX. Cross sections as high as 10^{-15} cm^2 are obtained for lines originating from $n = 3$ levels and they are more or less independent of the relative energy. This leads indeed to selective population of the $n = 3$ levels of beryllium-like Mg and thus accounts for the enhancement of the intensity of lines originated in these levels compared to other high-lying levels ($n \geqslant 4$). It is also noted that the intensity growth for these lines is prominent in the early stages; this is consistent with the expectation that at the beginning of the collision the plasmas interpenetrate and afterwards stagnate. We also observed an enhancement in intensity for all lines irrespective of their ionization state by a factor two at the red of the spectra, although theoretical calculations for charge exchange cross sections for these ions show values several orders lower than those for the lithium-like magnesium ion. So we expect that the enhancement in intensity of these lines is solely due to increase in electron density. This is supported by the fact that the enhancement in line intensities of Mg VIII and Mg VII is of the same scale as observed in the spectra.

4. Conclusions

XUV diagnostics of colliding laser-produced magnesium plasmas are performed. Pinhole photography and XUV spectroscopy are used as diagnostic tools. The time resolved photographic studies of colliding laser-produced magnesium plasmas give more insight into the expansion dynamics of the collision region. We investigated the possibility for the charge exchange collisions between lithium-like magnesium ions in a hot plasma and Mg V ions in a cold plasma. Enhanced line emission and continuum emission is observed from the collision region. The continuum suggests an increase of density leading to enhanced line intensities as indeed seen on all lines from Mg VII to Mg X. However, the highest increase among Mg IX lines

is for lines originated from $n = 3$ levels for which large charge exchange cross section are calculated. Hence we interpret this as selective population of $n = 3$ levels of beryllium-like magnesium ions due to charge exchange collisions. The true local enhancement of the lines will certainly be larger than that recorded. The time resolution of the present experiment is not fully adequate to study the dynamics of charge exchange collisions since perturbations in the population densities due to charge exchange collisions occur only during the short time of interpenetration.

Acknowledgment

One of us (SSH) thanks the Alexander von Humboldt foundation, Germany for a research fellowship.

References

[1] Chrisey D B and Hubler G K 1994 *Pulsed Laser Deposition of Thin Films* (New York: Wiley)
[2] Miller J C 1994 *Laser Ablation, Principles and Applications* (Heidelberg: Springer)
[3] Harilal S S, Bindhu C V, Nampoori V P N and Vallabhan C P G 1998 *Appl. Phys. Lett.* **72** 167
[4] Harilal S S, Radhakrishnan P, Nampoori V P N and Vallabhan C P G 1994 *Appl. Phys. Lett.* **64** 3377
[5] Harilal S S, Bindhu C V, Nampoori V P N and Vallabhan C P G 1998 *Appl. Phys.* B **66** 633
[6] Harilal S S 2001 *Appl. Surf. Sci.* **172** 103
[7] Park S M and Moon J Y 1999 *J. Appl. Phys.* **86** 7139
[8] Amoruso S, Bruzzese R, Spinelli N and Velotta R 1999 *J. Phys. B: At. Mol. Opt. Phys.* **32** R131
[9] Mah K W, Castro J, Costello J T, Kennedy E T, Lunney J G, McGlynn E, van Kampen P and Mosnier J P 2000 *Appl. Surf. Sci.* **168** 150
[10] Nakata Y, Kumuduni W K A, Okada T and Maeda M 1995 *Appl. Phys. Lett.* **66** 3206
[11] Hendron J M, Mahony C M O, Morrow T and Graham W G 1997 *J. Appl. Phys.* **81** 2131
[12] Issac R C, Harilal S S, Nampoori V P N and Vallabhan C P G 1998 *Appl. Phys.* A **67** 557
[13] Heald M A and Wharton C B 1965 *Plasma Diagnostics with Microwaves* (New York: Wiley)
[14] Schittenhelm H, Callies G, Berger P and Hugel H 1998 *Appl. Surf. Sci.* **129** 922
[15] Cameron S B, Tracy M D and Camacho J P 1996 *IEEE Trans. Plasma Sci.* **24** 45
[16] Harilal S S, Bindhu C V and Kunze H-J 2001 *J. Phys. D: Appl. Phys.* **34** 560
[17] Kunze H-J, Koshelev K N, Steden C, Uskov D and Wieschebrink H T 1994 *Phys. Lett.* A **193** 183
[18] Clark R W, Davis J, Velikovich A L and Whitney K G 1997 *Phys. Plasmas* **4** 3718
[19] Wan A S, Barbee T W Jr, Cauble R, Celliers P, Da Silva L B, Moreno J C, Rambo P W, Stone G F, Trebes J E and Weber F 1997 *Phys. Rev.* E **55** 6293
[20] Spicer D S, Clark R W and Maran S P 1990 *Astrophys. J.* **356** 549
[21] Galeev A A, Cravens T E and Gombosi T J 1985 *Astrophys. J.* **289** 807
[22] Farley D R, Estabrook K G, Glendinning S G, Glenzer S H, Remington B A, Shigemori K, Stone J M, Wallace R J, Zimmerman G B and Harte J A 1999 *Phys. Rev. Lett.* **83** 1982
[23] Shigemori K, Kodama R, Farley D R, Koase T, Estabrook K G, Remington B A, Ryutov D D, Ochi Y, Azechi H, Stone J and Turner N 2000 *Phys. Rev.* E **62** 8838
[24] Elton R C, Billings D M, Manka C K, Griem H R, Grun J and Ripin B H 1994 *Phys. Rev.* E **49** 1512
[25] Bosch R A, Berger R L, Failor B H, Delamater N D, Charatis G and Kauffman R L 1992 *Phys. Fluids* B **4** 979
[26] Henc-Bartolic V, Andreic Z, Gracin D, Aschke L, Ruhl F and Kunze H-J 1998 *Phys. Scr.* T **75** 297
[27] Ruhl F, Aschke L and Kunze H-J 1997 *Phys. Lett.* A **225** 107
[28] Stockl C and Tsakiris G D 1991 *Laser Part. Beams* **9** 725
[29] Chenais Popovics C *et al* 1997 *Phys. Plasmas* **4** 190
[30] Harilal S S, Bindhu C V and Kunze H-J 2001 *J. Appl. Phys.* **89** 4737
[31] Rancu O *et al* 1995 *Phys. Rev. Lett.* **75** 3854
[32] Shevelko V P 2000 *GSI Rep.* **2000–1** 115
[33] Tolstikhina Y and Shevelko V P 2000 *Short Commun. Phys. (Moscow)* **5** 46